

Soil moisture retrieval using reflection coefficients: numerical experiments

Alexander G. Voronovich and Richard J. Lataitis, *Senior Member, IEEE*

Abstract—Ready access to small, inexpensive, unmanned aerial vehicles (UAVs) allows for small-scale electromagnetic propagation and scattering experiments using airborne antennas. We consider a low-power, copter-mounted transmit antenna radiating at frequencies on the order of a hundred MHz, corresponding to wavelength on the order of meters, which at some horizontal distance generates a vertical interference pattern due to the interaction of a direct and ground-reflected wave. The depth of the interference fringes, which is directly related to the modulus of the soil reflection coefficient, can be measured by a second copter-mounted receiving antenna. By varying the geometry of the copter pair, and/or the transmitted signal frequency, the soil moisture profile up to a depth of a few meters can, in principle, be retrieved. In this paper we present the results of numerical experiments designed to evaluate the sensitivity of the angle- and frequency-dependence of the measured reflection coefficient to the soil moisture profile. Our simulations indicate that retrieval errors are small suggesting that the technique is feasible.

Index Terms—Geophysical measurement techniques, soil moisture

I. INTRODUCTION

The application of electromagnetic (EM) remote sensing techniques to the retrieval of land and vegetation parameters has a long history of scientific inquiry. Both monostatic and bistatic radar geometries have been considered. The scattered/reflected power of the radar signal generally depends on the characteristics of the vegetation, roughness of the surface, and moisture content of the soil. For sufficiently high-frequencies sub-surface inhomogeneities are also a factor [1]. When using polarimetric techniques the effects of surface roughness can be mitigated by computing a polarization ratio, which in the first approximation is independent of the surface roughness [2]. If vegetation effects can also be accounted for through auxiliary information, soil moisture can be retrieved. These retrievals typically invoke empirically established relations between measured and retrieved parameters [3], [4].

Bistatic geometries require both a transmitter and receiver and are often difficult and expensive to implement. The use of ground-reflected satellite signals from various global navigation satellite systems has proven to be a particularly appealing bistatic technique (GNSS-R) because of the widely and freely available GNSS “signals-of-opportunity” and ease of application. Most often Global Positioning Satellite (GPS) signals are used to retrieve soil moisture because of the sensitivity of their L-band operating frequency to soil water content. In addition, associated receivers can be easily mounted on a tower [5]-[9] or on an airplane [2], [10]-[13]. The similar retrieval of snow parameters was modelled [14] and successfully applied as well [15]. An in-depth review GNSS-R techniques can be found in [16], [17].

The reception of land-reflected signals by a second satellite is another geometry considered because of the potential of providing global coverage. This geometry was first successfully tested by the United Kingdom’s TDS-1 satellite [18]-[20]. The capabilities of this technique were significantly expanded with the launch in 2016 of a constellation of eight Cyclone Global Navigation Satellite System (CYGNSS) micro-satellites, which provided a very rich, high-time-resolution data set. Although intended for measuring tropical winds, CYGNSS also recorded land-reflections. Subsequent studies demonstrated that the measured land-reflected data could be used to retrieve soil moisture as well [21]-[22].

L-band signals, however, only penetrate into the soil to about 5 cm. In practice, soil moisture profiles to depths up to 1m and even deeper (i.e., the so-called root zone) are also of significant interest. This drew the attention of researchers to lower frequencies, in particular, to communication satellites operating in the P-band [15], [23]-[28]. Still, it is acknowledged in recent work [28] that “Although the P-band frequencies have a much larger penetration depth than the L-band, single-frequency data at the P-band is inadequate for the estimation of *root zone soil moisture (RZSM)*”.

In this paper we consider an alternative approach based on the broad availability of small, inexpensive, copter-type UAVs. By using a dual-UAV transmit-receive configuration the modulus of the soil reflection coefficient can be inferred from

This paragraph of the first footnote will contain the date on which you submitted your paper for review. It will also contain support information, including sponsor and financial support acknowledgment. For example, “This work was supported in part by the U.S. Department of Commerce under Grant BS123456.”

A. G. Voronovich, R. J. Lataitis, are with the Physical Sciences Laboratory of the NOAA Earth System Research Laboratories, 325 Broadway, Boulder, CO, 80305.

the measured interference pattern produced by a direct and ground reflected wave. Typical UAV separations and altitudes would be on the order of 100 *m*, and typical operating frequencies on the order 100 *MHz*. Transmitted signals at these frequencies can be made very narrow band, and, therefore, of very low-power with little chance of interfering with other man-made signals. This would allow for a more ready acquisition of permissions required to operate in this frequency band. Since the corresponding wavelengths used would be of the order of a few meters, the required accuracy of UAV locations would not be overly restrictive.

The use of a reflection mode (i.e., a bistatic radar) rather than a backscattering mode (i.e., the more traditional monostatic radar) coupled with relatively low frequencies offers significant advantages. Namely, the reflected signals become practically insensitive to surface roughness. The power loss of a specularly reflected signal is proportional to the square of the Rayleigh parameter, which is the ratio of wavelength to the RMS surface roughness height. For meter-long EM waves and centimeter-height soil roughness the Rayleigh parameter will be of the order of 10^{-4} - 10^{-3} . Since typical sizes and separations of leaves and branches are significantly smaller than the wavelength, the presence of vegetation can be accounted for as an effective dielectric layer with a possibly anisotropic tensor of effective dielectric permittivity. Therefore, in theory, vegetation parameters can be retrieved along with parameters of the soil.

In this paper the results of numerical simulations of the retrieval of soil moisture parameters based on the angle- and frequency-dependence of the soil reflection coefficient are presented. In general, the reflection coefficient is a complex quantity and measurements of its modulus and phase can be used, but phase measurements are particularly challenging and we consider retrieval algorithms based on knowledge of the modulus of the reflection coefficient only.

Let us assume that a transmitter (source S) and a receiver (R) are located at elevations z_S and z_R , respectively, and are separated by a horizontal distance r . The received signal will be the sum of a direct wave and a wave reflected from the soil. In what follows we assume that the boundary between the air and soil is strictly horizontal, and the properties of the soil are horizontally stratified. Thus, the surface roughness and possible horizontal inhomogeneities within the soil are neglected. The presence of vegetation can be also described in terms of a dielectric layer with an effective dielectric constant, and effectively be considered as a soil layer. Since the EM wavelengths under consideration will be relatively large, such assumptions should not be too unrealistic, at least to a first approximation. Variations of the soil properties with the vertical coordinate z are allowed, and retrieval of the dependence of dielectric constant of the soil on z represents the subject of this work. Because the dielectric constant $\epsilon(z)$ of soil (and vegetation) usually depends strongly on moisture, the information regarding $\epsilon(z)$ for a given type of soil (and vegetation) can be recast into the dependence of moisture on depth. For frequencies on the order of 100 *MHz* the penetration

of the EM field into the soil should be on the order of a few meters, and such a range of depths is of interest for many applications.

To a good approximation the total field ψ_{tot} at the receiver can be calculated in the geometric optics limit as the sum of the direct field ψ_{dir} and the field radiated by the mirror image of the source multiplied by the reflection coefficient $V(\theta)$ calculated for the corresponding incidence angle, that is, $\theta = \tan^{-1}(r/(z_R + z_S))$ and

$$\psi_{tot} = \psi_{dir}(r, z_R - z_S) + V(\theta)\psi_{dir}(r, z_R + z_S). \quad (1)$$

Here the air-soil boundary is located at $z = 0$. The direct field ψ_{dir} should be calculated, of course, with the directivity patterns of the receiver and transmitter included. When the coordinates of the transmitter and/or receiver vary on the order of a wavelength, the value of $|\psi_{tot}|$ will change due to phase variations of both ψ_{dir} terms in (1), however, small variations of the incident angle θ (and of the value of $V(\theta)$, correspondingly) can be neglected. In this case the ratio of the minimal to maximal value of $|\psi_{tot}|$:

$$\frac{|\psi_{tot}|_{min}}{|\psi_{tot}|_{max}} = \frac{\xi - |V(\theta)|}{\xi + |V(\theta)|} \quad \text{where} \quad \xi = \frac{|\psi_{dir}(r, z_R - z_S)|}{|\psi_{dir}(r, z_R + z_S)|} \quad (2)$$

defines the interference pattern. From this equation one can infer the reflection coefficient $|V(\theta)|$ from the depth of the interference pattern ξ . An error in calculating the angle θ will be on the order of the ratio of the error in determining UAV location to the characteristic distance between UAVs. If the former is on the order of a meter, the error in incidence angle will be of the order of one percent. On the other hand, one would like to avoid very small values of θ because when the distance between the transmitter and receiver is significantly smaller than the distance between receiver and the mirror image of the transmitter, the direct signal will dominate the reflected signal and the measurement of $|V(\theta)|$ will deteriorate.

Another option for measuring the depth of the interference pattern is to vary within narrow limits the frequency of the signal. If the characteristic distance between the receiver and the transmitter is L , then a variation of frequency on the order of

$$\Delta f \sim \frac{c}{L} \quad (3)$$

will also lead to a sequence of constructive and destructive interference of the two terms in (1). The variation of $|V(\theta)|$ within a relatively narrow frequency range can be neglected and $|V(\theta)|$ can again be determined from (2). For example, if $L \sim 100$ *m*, one finds $\Delta f \sim 3$ *MHz*, which is a reasonable frequency sweep bandwidth for practical applications.

In what follows we model the soil as a set of homogeneous dielectric layers. The complex dielectric constant ϵ of the layers strongly depends on their water content [29]-[31]. In [29] the following approximate formula was derived:

$$\epsilon = 3 + (56 + 7i)w \quad (4)$$

where w is a water content in g/cm^3 . Eq. (4) applies to soils like Manchester Fine Sand, Suffield Silty Clay, and some others, at temperatures above freezing as described in [29]. In [27] it was suggested that the moisture profile in the soil can be represented by a second-order polynomial: $w = az^2 + bz + c$. In this case our goal is to retrieve the numerical values of coefficients a , b , c . Other parametrizations of w were also considered in the literature, and in the general case our task is the retrieval of the associated soil moisture model parameters. Although some frequency (as well as temperature) dependence of the numerical parameters in (4) does exist, in this paper we investigate primarily the feasibility of retrieving the soil moisture profile using the angle- and frequency-dependence of the modulus of the soil reflection coefficient, and are not pursuing a detailed modeling of the dependence of the dielectric constant on water content.

When calculating the reflection coefficient we will be representing the soil as a stack of M sufficiently thin layers. The medium beneath the last (i.e., the M -th or deepest) layer is assumed to be a homogeneous half-space, and the medium above the first layer is assumed to be air with a dielectric constant of unity.

II. CALCULATION OF THE REFLECTION COEFFICIENT

Let us consider a downward-propagating EM plane wave of vertical or horizontal polarization incident on the stack of layers from the upper half-space at an incidence angle θ . The field within the n -th layer will be a superposition of two plane waves: one propagating downward with amplitude a_n and another wave propagating upward with amplitude b_n . The amplitudes of the waves will be considered in an “energy flux” normalization [32], in which the plane wave electric field \vec{E} can be expressed as:

$$\begin{aligned}\vec{E} &= a(k)q^{-1/2}(k)\vec{e}_-(k) \text{ or} \\ \vec{E} &= b(k)q^{-1/2}(k)\vec{e}_+(k),\end{aligned}\quad (5)$$

where k is the horizontal projection of the wave vector \vec{k} , and

$$q(k) = \left(\varepsilon \frac{\omega^2}{c^2} - k^2\right)^{1/2}, \quad \text{Im } q(k) \geq 0 \quad (6)$$

is the corresponding vertical projection, $\vec{e}_\mp(k)$ is a unit polarization vector for downward (-)/upward (+) propagation, and we assume $\text{Im } \varepsilon \geq 0$. The vertical component of the energy flux for the downward and upward propagating waves is given by $|a|^2$ and $|b|^2$, respectively.

The plane waves in all layers will have the same value k_0 of the horizontal projection of the wave vector defined by Snell’s Law: $k_0 = \omega \sin \theta / c$. Let us consider an individual boundary between two dielectric half-spaces with complex dielectric constants ε_1 (upper half-space) and ε_2 (bottom half-space). The Fresnel reflection (V) and transmission (T) coefficients with respect to the downward propagating wave in the first (top) half-space (i.e. the “ a_1 ” wave) can be expressed as [32]:

$$V = \frac{\varepsilon_2 q_1 - \varepsilon_1 q_2}{\varepsilon_2 q_1 + \varepsilon_1 q_2}, \quad T = \frac{2(\varepsilon_1 \varepsilon_2 q_1 q_2)^{1/2}}{\varepsilon_2 q_1 + \varepsilon_1 q_2}, \quad (7)$$

for VV (vertical) polarization and

$$V = \frac{q_1 - q_2}{q_1 + q_2}, \quad T = \frac{2(q_1 q_2)^{1/2}}{q_1 + q_2}, \quad (8)$$

for HH (horizontal) polarization. We note that V and T are generally complex and

$$V^2 + T^2 = 1. \quad (9)$$

Swapping indices $1 \leftrightarrow 2$ in (7) and (8), one can see that with respect to the wave incident from the bottom half-space onto the top half-space (i.e., the “ b_2 ” wave) the transmission coefficient is also T and the reflection coefficient becomes $-V$ (i.e., it changes sign). Based on the definition of reflection and transmission coefficients and using the superposition principle one can write:

$$\begin{aligned}b_1 &= V a_1 + T b_2 \\ a_2 &= T a_1 - V b_2,\end{aligned}\quad (10)$$

which, with the use of (9), becomes:

$$\begin{aligned}a_1 &= (a_2 + V b_2)/T, \\ b_1 &= (V a_2 + b_2)/T.\end{aligned}\quad (11)$$

Eq. (11) expresses the amplitudes of the waves above the boundary (a_1, b_1) in terms of the amplitudes (a_2, b_2) below it. In general, the amplitudes (a, b) of the waves at the lower boundary of a layer and the upper boundary of the layer differ by the phase propagation factor $\exp(\mp iqh)$, where h is the layer thickness. Therefore, one can evaluate the amplitudes by moving sequentially from the bottom layers upward, and the problem reduces to the following recursive equations:

$$\begin{aligned}a_n &= e^{-iq_n h_n} (a_{n+1} + V_n b_{n+1})/T_n, \\ b_n &= e^{+iq_n h_n} (V_n a_{n+1} + b_{n+1})/T_n,\end{aligned}\quad (12)$$

where V_n and T_n are the Fresnel reflection and the transmission coefficients, respectively, for the boundary between the n -th and the $(n+1)$ -th layers. The recursion starts from $a_{M+1} = 1, b_{M+1} = 0$ since in the lower half-space only the downward propagating wave is present. The last step of the recursion corresponds to $n = 0$ and represents the transition through the boundary between the top layer and the upper half-space (air). At this step one sets in (12) $h_0 = 0$. The resulting overall complex reflection coefficient from the stack of layers can be calculated as:

$$V(\theta) = b_0/a_0. \quad (13)$$

The procedure that was actually used in our calculations included a little refinement that does not alter the results but makes calculations more general. Namely, since the reflection coefficient $V(\theta)$ depends in fact only on ratio of amplitudes

(a, b) , one can at any step of the recursion multiply current amplitudes by the same factor without affecting $V(\theta)$. The first factor in (12), namely $e^{-iq_n h_n}$, for very thick layers or very high frequencies may become exponentially large. To avoid possible numerical overflow, we multiply both equations in (12) by $e^{iq_n h_n}$. Thus, the recursion relation actually used in our calculations is given by:

$$\begin{aligned} a_n &= (a_{n+1} + V_n b_{n+1})/T_n, \\ b_n &= e^{2iq_n h_n} (V_n a_{n+1} + b_{n+1})/T_n. \end{aligned} \quad (14)$$

This recursion prevents exponentially large factors, but may include exponentially small ones, which does not present a problem.

III. SOLUTION OF THE INVERSE PROBLEM

Let the square modulus of the reflection coefficient measured at a number of incidence angles θ_a , $a = 1, 2, \dots, A$ and a set of frequencies f_b , $b = 1, 2, \dots, B$ be denoted by $\tilde{R}_{a,b}$. The solution of the inverse problem can be posed as a minimization with respect to the parameters of a model p_i of the following norm:

$$N(p_i) = \frac{1}{AB} \sum_{b=1}^B \sum_{a=1}^A (R(\theta_a, f_b; p_i) - \tilde{R}_{a,b})^2, \quad (15)$$

where

$$R(\theta_a, f_b; p_i) = |V(\theta_a, f_b; p_i)|^2, \quad (16)$$

and the reflection coefficient $V(\theta_a, f_b; p_i)$ is calculated for a given set of parameters p_i according to the algorithm presented in the previous section. This norm characterizes the mismatch between the measured and theoretically calculated values of the reflection coefficient at points in the parameter space.

The minimization of the norm $N(p_i)$ with respect to the parameters p_i is accomplished through two steps. The first consists of an approximate retrieval. The limits within which the parameters are expected to lie and uniform intervals between the limits are defined to form a set of gridded points spanning the parameter space. The norm (15) is then calculated at each point and local minima evaluated. These local minima become the first-guess (starting) points of the second step, which represents a “refined” search. In our calculations we use 15 uniformly-spaced points spanning the defined parameter limits.

The refined search proceeds iteratively and is based on a calculation of the gradient vector $\partial N/\partial p_i$ of the norm and corresponding Hessian matrix $\partial^2 N/\partial p_i \partial p_j$ at the starting point. The gradient vector and the eigenvectors of the Hessian matrix generate a set of optimal directions (i.e., 1D manifolds) along which the minimization of the norm is accomplished, which is a straightforward process. From the resulting set of local minima locations the point with the overall minimum value is chosen. This point is set as the new starting point and

the procedure repeated. Iterations stop when the value of the norm ceases to decrease or the location of the point minimizing the norm does not change appreciably. This procedure appears to be rather robust and usually works well even for multidimensional parameter spaces. Its practical drawback is the need to be able to calculate the gradient and the Hessian matrix analytically. This task can be rather laborious, but is doable. By differentiating equations (14) with respect to the parameters p_i one obtains equations in terms of the corresponding derivatives $\partial a_n/\partial p_i$, $\partial b_n/\partial p_i$ (and similarly for the second derivatives). These derivatives can be calculated recursively in a manner similar to the calculation of the amplitudes (a, b) themselves.

IV. NUMERICAL SIMULATIONS

In this section the following three-parameter Gaussian model of soil moisture profile is considered:

$$w(z) = w_{max} \exp\left(-\frac{(z-z_{max})^2}{d^2}\right), \quad (17)$$

where $0 < w_{max} < 1$ is the maximum value of water content at $z = z_{max}$ and d is the width of the profile. If $z_{max} > 0$, the maximum is reached within the soil, otherwise the water content monotonously decreases with increase of depth $z > 0$. The set of parameters p_i for this model consists of only three members: $p_1 = w_{max}$, $p_2 = z_{max}$, and $p_3 = d$.

For a case study we consider the following simulation parameters: $w_{max} = 0.35 \text{ g/cm}^3$ and $z_{max} = d = 0.2 \text{ m}$. In what follows we will refer to these as “actual” values. This profile was represented in our simulations as a set of $n_L = 10$ layers of 0.05 m width each, and is depicted in Fig. 1 by the solid line. At depths $z > 0.5 \text{ m}$ the water content was assumed to be a constant corresponding to the lowest point of the profile.

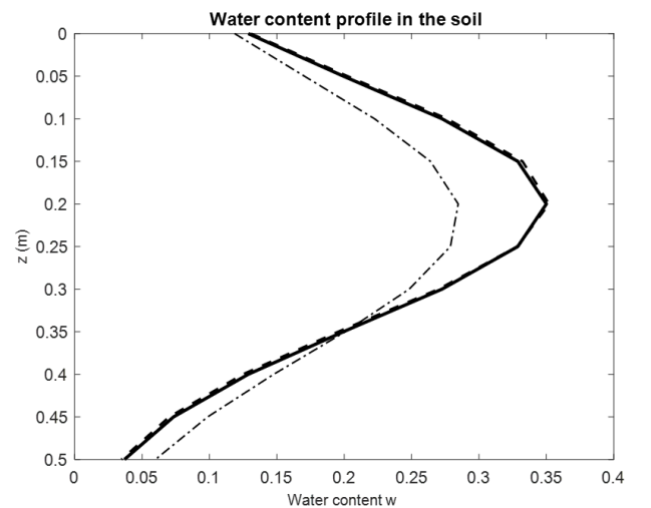


Figure 1. Water content profile in the soil. Solid line – actual profile; dash-dot line – approximate retrieval; dashed line – refined retrieval.

The frequency dependence of the reflection coefficient for this model calculated for an incidence angle $\theta = 45^\circ$ for both vertical (VV) and horizontal (HH) polarizations is shown in Fig.2. It was assumed that the square modulus of the reflection coefficient at vertical polarization is given (was “measured”) at a set of incidence angles ranging from 10° to 70° with a 0.5° step at three frequencies: $f = 100, 125,$ and 150 MHz (121×3 values altogether).

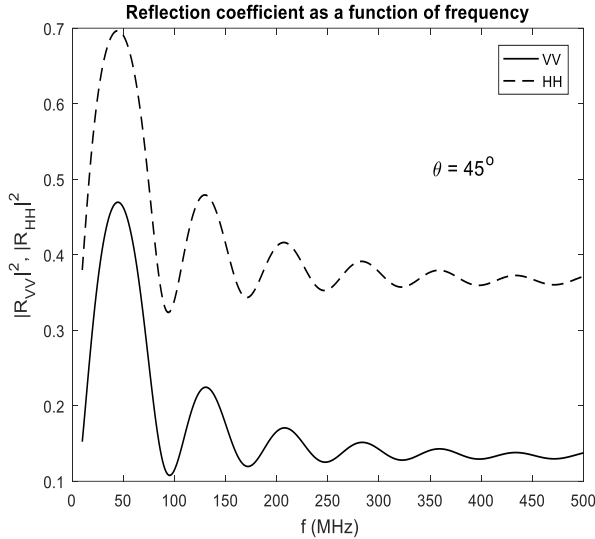


Figure 2. Frequency dependence of the reflection coefficients.

To increase penetration of the EM radiation into the soil one might be tempted to use lower frequencies. One has to keep in mind, however, that this will concurrently reduce the depth resolution. We also avoided using very small grazing angles because this will significantly reduce the horizontal spatial resolution, which is nominally of the order of the size of the first Fresnel zone: $((L\lambda)^{1/2} \sim (100 \cdot 3)^{1/2} \text{ m} \sim 15 \text{ m})$.

The penetration of the field into the soil is shown in Fig. 3.

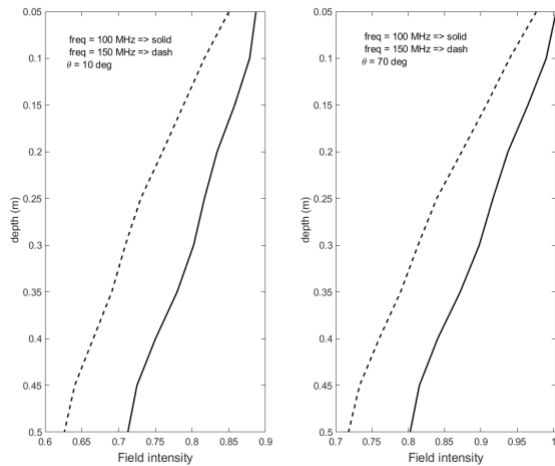


Figure 3. Penetration of the field into the soil. The left plot corresponds to an incidence angle of 10° and the right to an incidence angle of 70° . The solid line represents a frequency $f = 100 \text{ MHz}$ and dashed line $f = 150 \text{ MHz}$.

Note that field intensity in the figure corresponds to the square modulus of the amplitudes of the upward- and downward-propagating waves $|a|^2 + |b|^2$ in a layer normalized by the amplitude of incident field in the air. One can see that the field penetrates relatively deeply into the soil.

In the absence of noise it is not too difficult to retrieve profile parameters precisely (at least when the first-guess point of the refined search in the parameter space is not too far away from the precise one). This is, however, a so-called “inverse crime” that poorly represents practical situations. For this reason we artificially distorted the simulated data by adding random, multiplicative, uncorrelated “noise” replacing the actual values of the complex reflection coefficient R according to the following formula: $R \rightarrow R \cdot (1 + n_L \cdot \eta)$, where η are random complex numbers with real and imaginary parts uniformly and independently distributed within the interval $(-1,1)$ and n_L being a real factor that we will be referring to as a “noise level”. For the following simulations we selected the noise level to be 0.1 (i.e. 10%). The resulting data are represented by the dots in Fig. 4. The approximate retrieval used the following set of parameter ranges: $0 < w_{max} < 1$, $-0.5 \text{ m} < z_{max} < 0.5 \text{ m}$, $0.1 \text{ m} < d < 1 \text{ m}$.

Three first-guess (starting) points of the refined search led to the same retrieved parameters that are shown in Table 1. One can see that the retrieval appears to be of good quality.

Table 1	w_{max}	z_{max}	d
actual values	0.35	0.2 m	0.2 m
retrieved values	0.3520	0.1977 m	0.1986 m
error	0.57%	1.12%	0.70%

This numerical experiment was repeated for the case of horizontal polarization using the same set of parameters. The field penetration into the soil and the results of the approximate retrieval are quite similar to the case of vertical polarization. The angular dependencies of the square modulus of the reflection coefficients are shown on Fig. 5. As before, all three first-guess points lead to the same retrieved parameters shown in Table 2. The quality of the retrieval is slightly worse but comparable to the case of vertical polarization.

Table 2	w_{max}	z_{max}	d
actual values	0.35	0.2 m	0.2 m
retrieved values	0.3707	0.1949 m	0.1894 m
error	5.91%	2.55%	5.30%

As mentioned above, the calculation of the reflection coefficient requires measurements of the depth of the interference pattern formed by the direct and reflected waves, which requires either varying the distance between the transmitter and the receiver, or, if both are sufficiently far apart (i.e., a large enough L in (3)), varying within relatively narrow limits the carrier frequency. Such a procedure might be somewhat impractical, and it may be of interest to try to use instead of the square modulus of the reflection coefficient the square modulus of the total field measured at a set of points

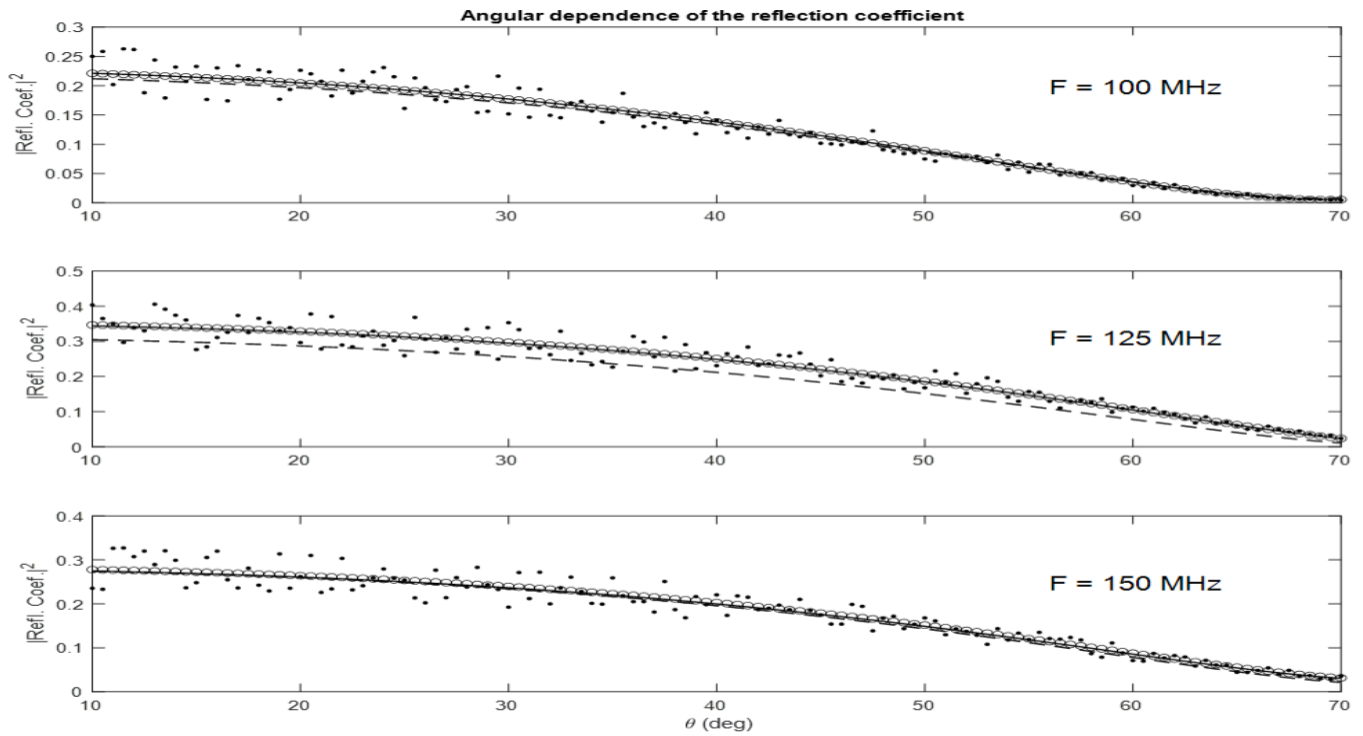
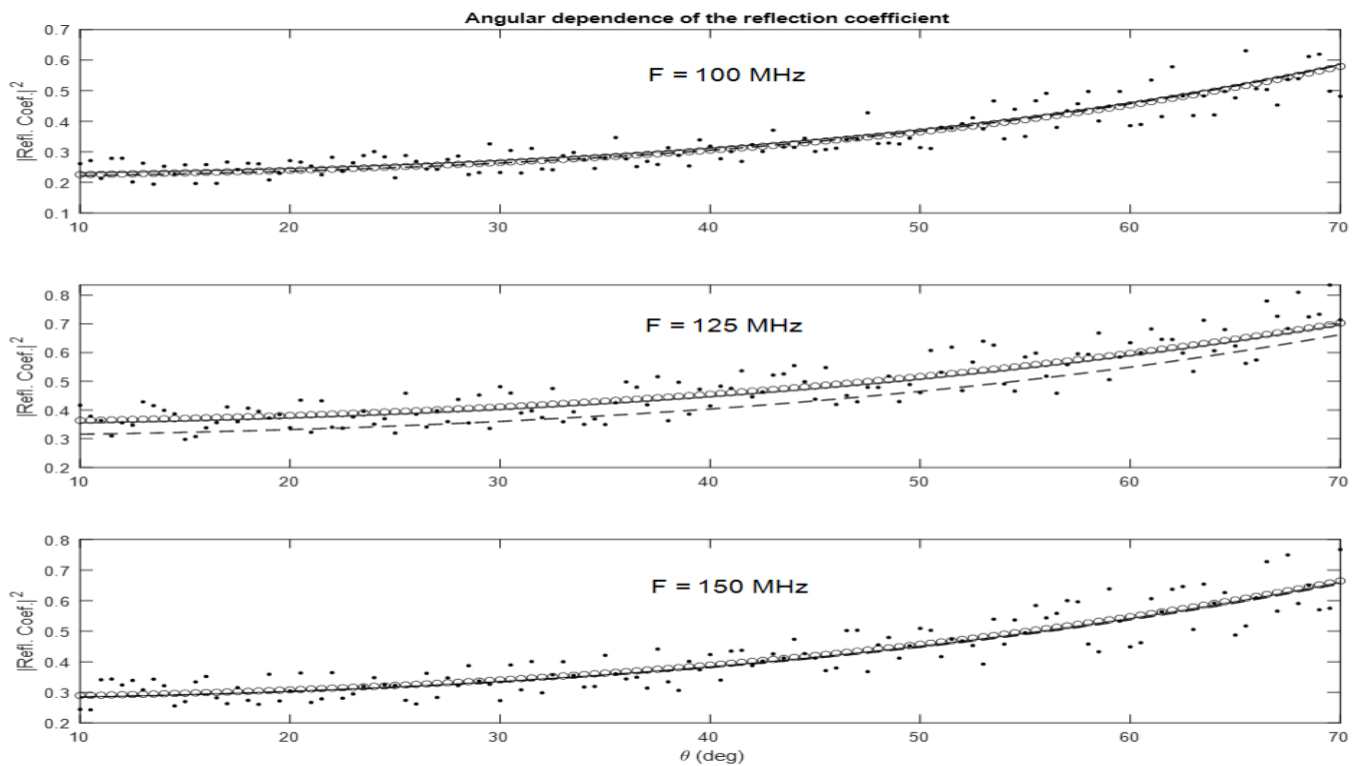


Figure 4 (upper). The angular dependence of the square modulus of the reflection coefficient. The dots represent “noisy” data used in the retrieval, the dashed line corresponds to the approximate retrieval, and the circles to the refined retrieval. Actual values (i.e., without noise) are shown as solid lines.

Figure 5 (lower). The same as Fig. 4 but for horizontal polarization. The dots represent “noisy” data used in the retrieval, the dashed line corresponds to the approximate retrieval, and the circles to the refined retrieval. Actual values (i.e., without noise) are shown as solid lines.



with known coordinates (i.e., the total field given by (1)). It is convenient to normalize this field by the direct field radiated by the mirror image of the source, which gives:

$$|\tilde{\psi}_{tot}|^2 = \left| \frac{\psi_{dir}(r, z_R - z_S)}{\psi_{dir}(r, z_R + z_S)} + V(\theta) \right|^2. \quad (18)$$

We tried this approach by repeating our numerical simulations for the same model of soil moisture. We assumed that the source was located at a height of $z_S = 10$ m and the receiver at a height $z_R = 20$ m. The horizontal separation r varied between 5.3 m and 82.4 m, which corresponds to the same range of incidence angles 10° - 70° . The total field intensity was also evaluated at the same number of uniformly distributed horizontal points. The level of multiplicative noise was set at 5% (by a factor of two less than before). Results are shown in Fig. 6.

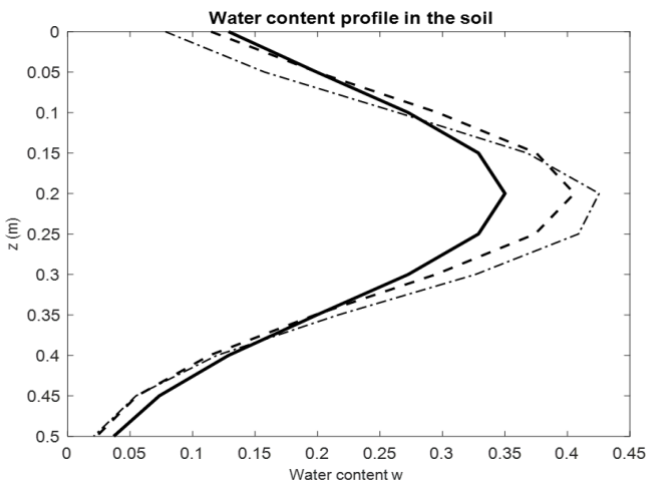


Figure 6. The same as Fig. 1 but using the squared modulus of the normalized total field. Solid line – actual profile; dash-dot line – approximate retrieval; dashed line - refined retrieval.

The results of the retrieval performed for horizontal polarization is shown in Table 3. The quality of the retrieval significantly deteriorated. This happens in spite of the seemingly very good match of the total field achieved for all frequencies shown in Fig. 7. We suggest the reason for this discrepancy is that the value of the reflection coefficient in (18) is now masked by the first term (the ratio of direct fields), and the 5% multiplicative noise overwhelms the contribution from the reflection coefficient. This becomes even more pronounced with respect to vertical polarization, for which the reflection coefficient has smaller values for large incidence angles. For this reason simulated retrievals for vertical polarization produced even worse results than those shown in Table 3.

Table 3	w_{max}	z_{max}	d
actual values	0.35	0.2 m	0.2 m
retrieved values	0.4055	0.1996 m	0.1776 m
error	15.9 %	0.2 %	11.2 %

The only case considered so far is well suited for a theoretical

evaluation of the retrieval procedure because it includes both a significant variation in water content and it has a non-monotonic dependence on depth. Such a profile is not, however, typical in practice. In [27] a second-order polynomial approximation for the depth dependence of water content was considered with references to experimental results. Such an approximation follows from (17) for sufficiently large d . In Fig. 8 two such cases are considered with monotonously varying water content. In cases (a),(b) as before three frequencies and a 10% noise level were used. One can see that the retrieval of deeper moisture levels is less accurate. If, however, two more frequencies are added (112.5 and 137.5 MHz: see case (c)), the quality of retrieval improves. It is interesting that in the case of the profile shown in (b),(c) a strong dependence of the quality of retrieval on noise level was observed: for a noise level of 2.5% the retrieval becomes practically exact; however, for a noise level of 3% the retrieval deteriorates significantly.

V. DISCUSSION

We have explored the feasibility of retrieving soil moisture profiles using the dependence of the square modulus of the reflection coefficient on the incidence angle measured at a few frequencies. The soil moisture profile was parametrized by a Gaussian curve described by three parameters: the maximum value of soil moisture, its depth, and the width of the profile. A case study of a retrieval carried out in the presence of random multiplicative noise yielded good results with retrieval errors not exceeding a few percent for both vertical and horizontal polarizations.

The retrieval based on measurements of the normalized intensity of total field instead of square modulus of the reflection coefficient produced significantly worse results. The most likely reason is that the dynamic range of the interference pattern itself is much higher than the dynamic range of the variations of the reflection coefficient, and the same level of multiplicative noise masks variations that are due to the angular dependence of the reflection coefficient. Fig. 7 shows the dependence of the squared modulus of the total normalized field as a function of transmitter and receiver separation for three different frequencies.

The results presented in Fig. 7 pose the following question: Why does the seemingly perfect match of the actual and retrieved fields still lead to a poor retrieval of the moisture profile? The same question applies to Fig. 4. Why do the actual (solid line) and retrieved angular dependence of the reflection coefficient corresponding to the approximate retrieval for $f = 100$ MHz and $f = 150$ MHz (dashed line) agree so well while the approximate profile retrieval depicted in Fig. 1 (dash-dot line) differs so significantly from the actual profile (solid line)?

We suggest that this apparent anomaly is due to the relatively high value of the dielectric constant of the soil, which results in an angular dependence of the reflection coefficient that is mostly due to the high contrast between the dielectric constant of air and top level of the soil. Below we consider this issue in more detail.

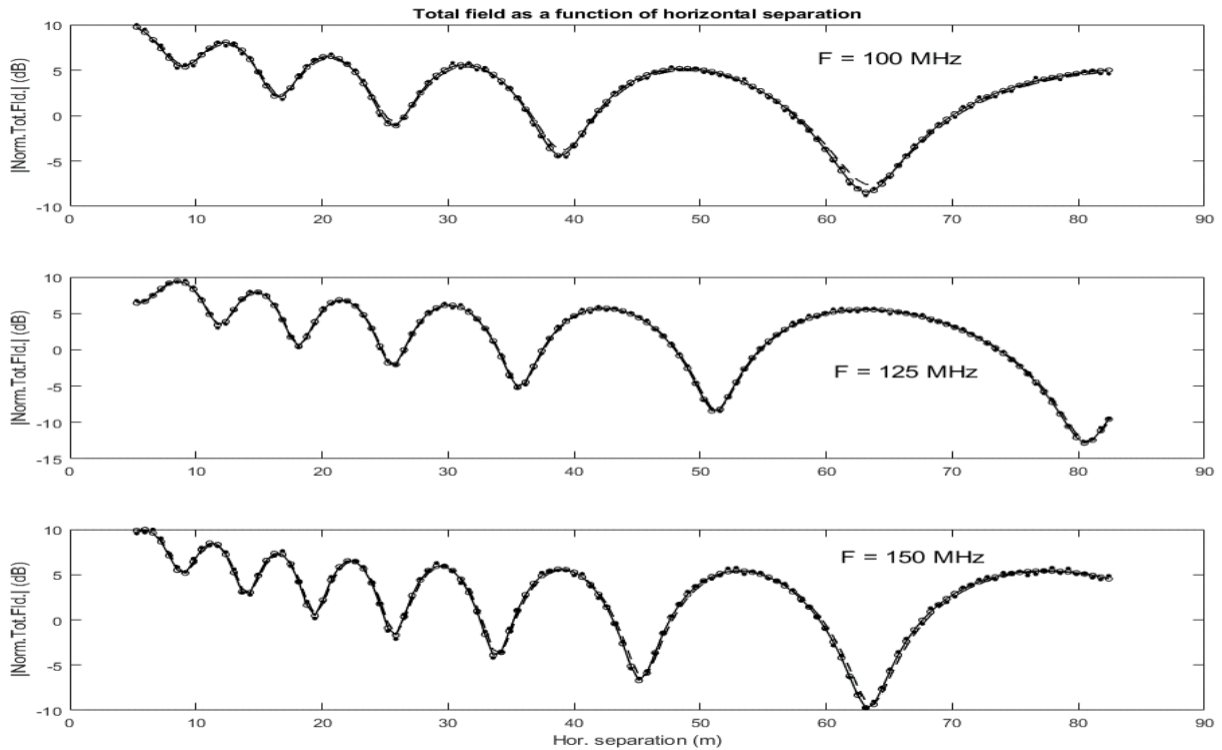
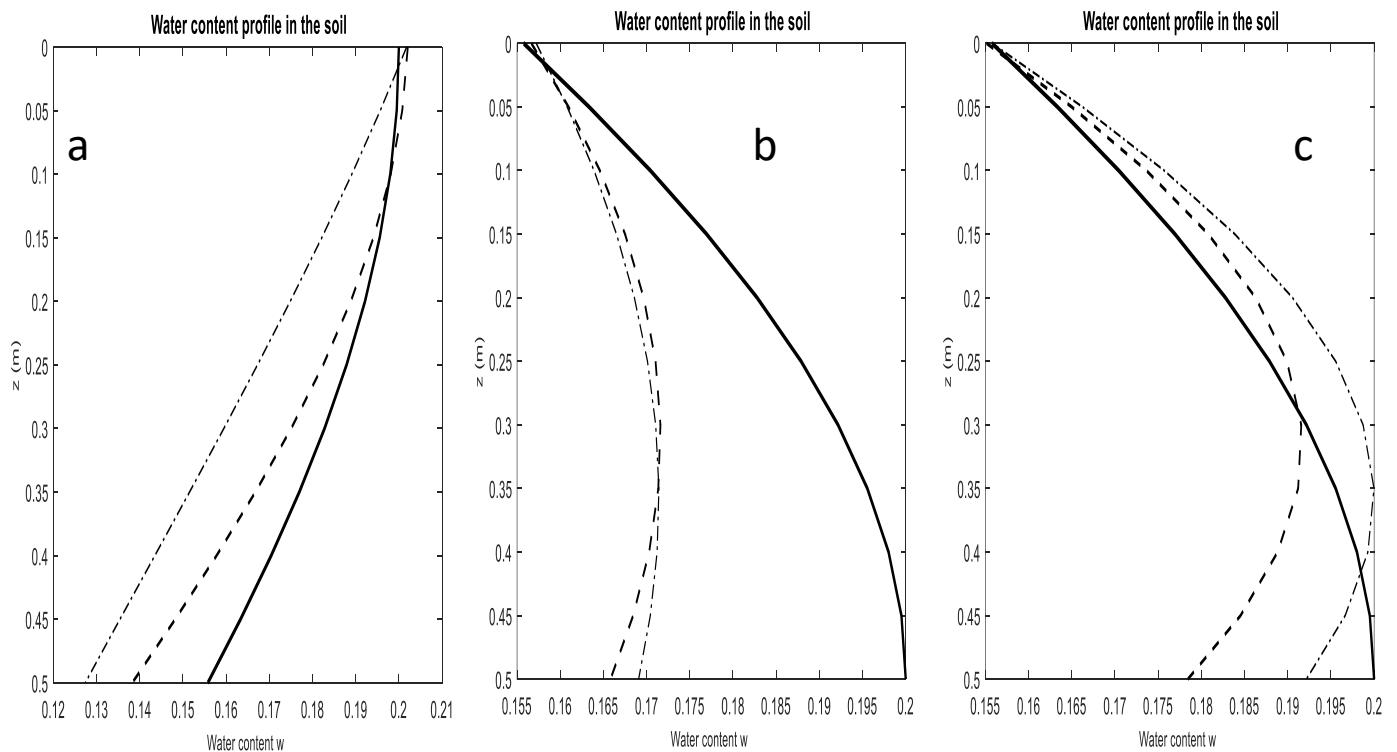


Figure 7 (upper). The dependence of the square modulus of the total field in dB on horizontal separation. The actual and retrieved values are represented by the solid line and circles, respectively. As in Fig. 4 and 5 the dots represent the “noisy” data used in the retrieval. They are less evident here because of the dB scale used.

Figure 8 (lower). The same as Fig. 1 but using different soil moisture profile parameters: (a) $z_{max} = 0$; (b,c) $z_{max} = 0.5$ m. In all cases $w_{max} = 0.2$, $d = 1$ m, and the noise level was 10 %. In cases (a,b) three frequencies: 100, 125, and 150 MHz were used for the retrieval, and in case (c) two more frequencies: 112.5 and 137.5 MHz were added. Solid line – actual profile; dash-dot line – approximate retrieval; dashed line - refined retrieval.



Due to Snell's Law the incidence angle θ_n for waves propagating in the n -th layer within the soil is given by:

$$\sin\theta_n = \frac{\sin\theta}{\sqrt{\epsilon_n}}, \quad (19)$$

where θ is the incidence angle in the air (a consequence of the conservation of the horizontal component of the wave vector). For large $|\epsilon_n| \gg 1$ the incidence angles θ_n become small (i.e., the waves in the soil propagate nearly vertically regardless of the value of incidence angle in the air θ) and the ratio v_1 of amplitudes of up-to-down propagating waves immediately below the boundary between the air and the soil ($v_1 = b_1/a_1$) only weakly depends on θ . Eq. (12) for the boundary between air and soil becomes:

$$\begin{aligned} a_0 &= (a_1 + V_F b_1)/T_F, \\ b_0 &= (V_F a_1 + b_1)/T_F, \end{aligned} \quad (20)$$

where $V_F = V_F(\theta)$ is the Fresnel reflection coefficient for the boundary between the air and the first layer in the soil. From (20) one finds:

$$V(\theta) = \frac{b_0}{a_0} = \frac{V_F(\theta) + v_1}{1 + V_F(\theta)v_1}, \quad (21)$$

where $V(\theta)$ is the overall reflection coefficient from the full set of dielectric layers within the soil. For $|\epsilon_n| \gg 1$ one obtains from (7) for vertical polarization:

$$V_F(\theta) = \frac{\epsilon \cos\theta - \sqrt{\epsilon - \sin^2\theta}}{\epsilon \cos\theta + \sqrt{\epsilon - \sin^2\theta}} \approx \frac{\sqrt{\epsilon} \cos\theta - 1}{\sqrt{\epsilon} \cos\theta + 1}, \quad (22)$$

and from (8) for horizontal polarization:

$$V_F(\theta) = \frac{\cos\theta - \sqrt{\epsilon - \sin^2\theta}}{\cos\theta + \sqrt{\epsilon - \sin^2\theta}} \approx \frac{\cos\theta - \sqrt{\epsilon}}{\cos\theta + \sqrt{\epsilon}}. \quad (23)$$

In both cases one obtains from (21):

$$V(\theta) \approx \frac{\cos\theta - \chi_0}{\cos\theta + \chi_0}, \quad (24)$$

where:

$$\chi_0 = \frac{1 - v_1}{\sqrt{\epsilon} + v_1}, \quad \chi_0 = \sqrt{\epsilon} \frac{1 - v_1}{1 + v_1}, \quad (25)$$

are weakly dependent function of θ for both vertical and horizontal polarizations, respectively.

Fig. 9 depicts the angular dependence of the square modulus of the reflection coefficient calculated exactly (solid lines) and according to the approximate asymptotic expression (24) with χ_0 set to a constant (dash lines). One can see that the difference between the two results is rather small for both polarizations. However, it is this difference that carries information about the profile of the dielectric constant in the soil. The bulk of the angular dependence is due to the large contrast between dielectric constants of the air and soil. Thus, retrieval of the moisture profiles based on the angular dependence of the reflection coefficient is more difficult for soils with large dielectric constants.

We note that χ_0 , which is only weakly dependent on θ , depends nevertheless on frequency. This dependence for both polarizations is shown on Fig. 10. Thus, the weak dependence of the reflection coefficient on dielectric constant profile observed for high ϵ can be mitigated, if necessary, by measurements using a sufficiently broad set of frequencies.

To ensure deeper penetration of the EM radiation into the soil one may try using even lower frequencies. It has to be kept in mind, however, that in this case vertical resolution of soundings will also degrade and some optimal trade off should exist. The same applies to the range of incidence angles: too large a θ will significantly increase the Fresnel zone size and correspondingly reduce the horizontal resolution.

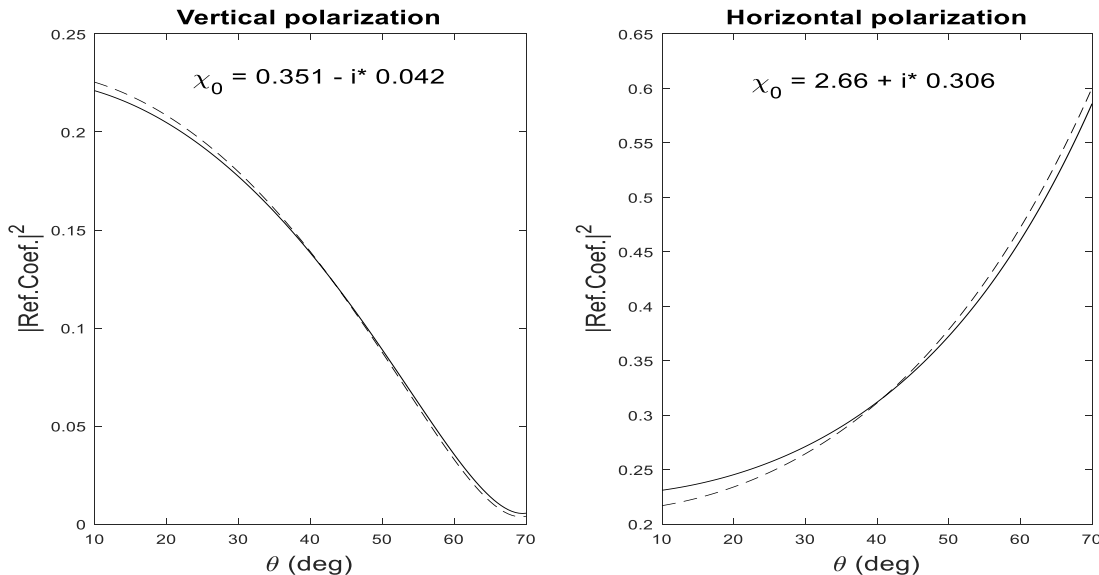


Figure 9. Angular dependence of the reflection coefficient calculated exactly (solid lines) and according to the asymptotic result given by (24) (dashed lines).

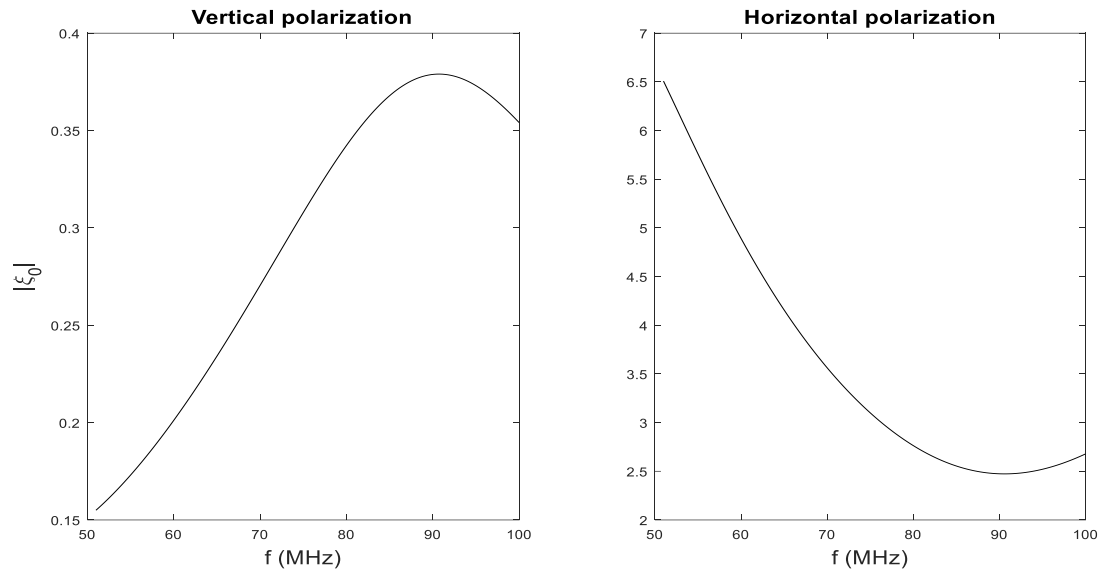


Figure 10. The dependence of the modulus of the parameter χ_0 on frequency.

VI. ACKNOWLEDGEMENTS

The authors would like to thank the reviewers for their many helpful comments, and, in particular, Dr. Valery Zavorotny, for many useful discussions. This work was supported by the NOAA Physical Sciences Laboratory.

VII. REFERENCES

- [1] S. Zwieback et al, “Depth-Resolved Backscatter and Differential Interferometric Radar Imaging of Soil Moisture Profiles: Observations and Models of Subsurface”, *IEEE J. Sel. Topics in Appl. Earth Obs. Remote Sens.*, v. 10 (7) pp. 3281-3296, (2017).
- [2] Egido, A., S. Paloscia, E. Motte, L. Guerriero, N. Pierdicca, M. Caparrini, E. Santi, G. Fontanelli, and N. Floury, “Airborne GNSS-R polarimetric measurement for soil moisture and above ground biomass estimation,” *IEEE J. Selected Topics in Applied Earth Observations and Remote Sens.*, v. 7 (5), pp. 1522-1532, (2014).
- [3] D. Entekhabi et al., “The Soil Moisture Active Passive (SMAP) Mission”, *Proc. IEEE*, v. 98 (5), pp. 704-716, (2010).
- [4] V. Naeimi et al, “An Improved Soil Moisture Retrieval Algorithm for ERS and METOP Scatterometer Observations”, *IEEE Trans. Geosci. Remote Sens.*, v. 47 (7), pp. 1999-2013, (2009).
- [5] Zavorotny, V., K. Larsen, J. Braun, E. Small, E. Gutmann, and A. Bilich, “A physical model for GPS multipath caused by land reflections: Toward bare soil moisture retrievals,” *IEEE J. Selected Topics in Applied Earth Observations and Remote Sens.*, v. 3 (1), pp. 100-110, (2010).
- [6] A. Arroyo et al, “Dual-Polarization GNSS-R Interference Pattern Technique for Soil Moisture Mapping”, *IEEE J. Sel. Topics in Appl. Earth Obs. Remote Sens.*, v. 7 (5) pp. 1533-1543, (2014).
- [7] A. Egido et al, “Global Navigation Satellite Systems Reflectometry as a Remote Sensing Tool for Agriculture”, *Remote Sensing*, v. 4, pp. 2356-2372, (2012).
- [8] N. Pierdicca et al, “SAVERS: A Simulator of GNSS Reflections from Bare and Vegetated Soils”, *IEEE Trans. Geosci. Remote Sens.*, v. 52 (10), pp. 6542-6554, (2014).
- [9] N. Rodriguez-Alvarez et al, “Land Geophysical Parameters Retrieval Using the Interference Pattern GNSS-R Technique”, *IEEE Trans. Geosci. Remote Sens.*, v. 49 (1), pp. 71-84, (2011).
- [10] Katzberg, S., O. Torres, M. S. Grant, and D. Masters, “Utilizing calibrated GPS reflected signals to estimate soil moisture reflectivity and dielectric constant: Results from SMEX02,” *Remote Sens. Environment*, v. 100, pp. 17-28, (2005).
- [11] N. Ye et al, “Airborne P-band passive microwave soil moisture remote sensing: preliminary results”, *Proc. IGARSS*, pp. 6223-6226, (2019).
- [12] M. Gamba et al., “Prototyping a GNSS-Based Passive Radar for UAVs: An Instrument to Classify the Water Content Feature of Lands”, *Sensors*, v. 15, pp. 28287-28313, (2015).
- [13] E. Motte et al, “GLORI: A GNSS-R Dual Polarization Airborne Instrument for Land Surface Monitoring”, *Sensors*, v.16, 732, (2016).
- [14] S. Yueh et al, “Remote Sensing of Snow Water Equivalent Using Coherent Reflection from Satellite Signals of Opportunity: Theoretical Modeling”, *IEEE J. Sel. Topics in Appl. Earth Obs. Remote Sens.*, v. 10 (12), pp. 5529-5540, (2017).
- [15] Shah, R., X. Xu, S. Yueh, C.-S. Chae, K. Elder, R. Starr, and Y. Kim, “Remote sensing of snow water equivalent using P-band coherent detection”, *IEEE Geosci. Remote Sens. Lett.*, v. 14 (3), pp. 309-313, (2017).
- [16] V. Zavorotny et al, “Tutorial on Remote Sensing Using GNSS Bistatic Radar of Opportunity”, *IEEE Geosci. Remote Sens. Mag.*, v.2 (4), pp. 8-45, (2014).
- [17] S. Gleason, S. Lowe, and V. Zavorotny, “Remote Sensing with Bistatic GNSS Reflections”, Chapter in *GNSS Applications and Methods*, Eds. S. Gleason and D. Gebre-Egziabher, Artech House, 2009, ISBN 978-0-472-11935-6.
- [18] A. Camps et al, “Sensitivity of GNSS-R Spaceborne Observations to Soil Moisture and Vegetation”, *IEEE J. Sel. Topics in Appl. Earth Obs. Remote Sens.*, v. 9 (10) pp. 4730-4742, (2016).
- [19] C. Chew et al, “Demonstrating soil moisture remote sensing with observations from the UK TechDemoSat-1 satellite mission”, *Geophys. Res. Letters*, v. 43, pp. 3317-3324, (2016).
- [20] A. Camps et al, “Sensitivity of TDS-1 GNSS-R Reflectivity to Soil Moisture: Global and Regional Differences and Impact of Different Spatial Scales”, *Remote Sensing*, 10, 1856, (2018).
- [21] C. Chew and E. Small, “Soil Moisture Sensing Using Spaceborne GNSS Reflections: Comparison of CYGNSS Reflectivity to SMAP Soil Moisture”, *Geophys. Res. Letters*, v. 45, pp. 4049-4057, (2018).
- [22] M. Al-Khaldi et al, “Time-Series Retrieval of Soil Moisture Using CYGNSS”, *IEEE Trans. Geosci. Remote Sens.*, v. 57 (7), pp. 4322-4331, (2019).
- [23] S.H. Yueh, X. Xu, R. Shah, S. Margulis, and K. Elder, “P-band signals of opportunity for remote sensing of root zone soil moisture”, *Proc. IGARSS*, pp. 1403-1406, (2018).

- [24] J.L. Garrison, M. Kurum, B. Nold, J. Piepermeier, M.A. Vega, R. Bindlish and G. Pignotti, "Remote sensing of root-zone soil moisture using I- and P-band signals of opportunity: instrument validation studies", Proc. IGARSS, pp. 8314-8317, (2018).
- [25] J. L. Garrison, B. Nold, Y.-C. Lin, G. Pignotti, J. R. Piepermeier, M. Vega, M. Fritts, C. DuToit, and J. Knuble, "Recent results on soil moisture remote sensing using P-band signals of opportunity," in IEEE International Conference on Electromagnetics in Advanced Applications (ICEAA), pp. 1604-1607, (2017).
- [26] J. L. Garrison, Y-C Lin, B. Nold, J. R. Piepermeier, M. A. Vega, M. Fritts, C. F. duToit, and J. Knuble, "Remote sensing of soil moisture using P-band signals of opportunity (SoOp): Initial results," in IEEE International Conference on Electromagnetics in Advanced Applications (ICEAA), pp. 4158-4161, (2017).
- [27] A. Tabatabaenejad, M. Burgin, X. Duan, and M. Moghaddam, "P-band radar retrieval of subsurface soil moisture profile as a second-order polynomial: First AirMOSS Results", IEEE Trans. On Geoscience and Remote Sensing, v. 53 (2), pp. 645-658, (2015).
- [28] S. Yueh et al, "Experimental Demonstration of Soil Moisture Remote Sensing Using P-Band Satellite Signals of Opportunity", IEEE Geosci. Remote Sens. Lett., v. 17 (2), pp. 207-211, (2020).
- [29] P. Hoekstra and A. Delaney, "Dielectric properties of soils at UHF and microwave frequencies", J. Geophys. Res., v. 79 (11), pp. 1699-1708, (1974).
- [30] N.R. Peplinski, F.T. Ulaby, and M.C. Dobson, "Dielectric properties of soils in the 0.3-1.3 GHz range", IEEE Trans. Geosci. Remote Sensing, v. 33 (3), pp. 803-807, (1995).
- [32] V.L. Mironov, L.G. Kololapova, and S.V. Fomin, "Physically and mineralogically based spectroscopic dielectric model for moist soils", IEEE Trans. Geosci. Remote Sensing, v. 47 (7), pp. 2059-2070, (2009).
- [32] A.G. Voronovich, "Small-slope approximation for electromagnetic wave scattering at a rough interface of two dielectric half-spaces", Waves in Random Media, v. 4, pp. 337-367, (1994).